Master of
Science Thesis
VT2019

# Iodine Quantification Using Dual Energy Computed Tomography and applications in Brain Imaging

---


Veronica Fransson

Supervision

Kristina Ydström

Department of Medical Radiation Physics,
Clinical Sciences, Lund
Lund University

# Med Dual Energy-teknik förs forskningen inom röntgen framåt

Att man kan använda röntgenstrålning för att ta bilder på kroppens inre har varit känt sedan sent 1800-tal och idag finns det en mängd olika röntgenapparater. En sådan är datortomografen, computed tomography (CT) på engelska. Med datortomografi är det möjligt att avbilda patienten i tre dimensioner, istället för vid slätröntgen där man endast får ut en tvådimensionell bild. Detta möjliggör en bättre visualisering och diagnostisering av sjukdomar och skador. Detta, plus dess snabbhet och tillgänglighet, har gjort att antalet datortomografiska undersökningar i Sverige ökat flera gånger om sedan mitten av 90-talet.

Beroende på vilken röntgenenergi som används kan olika vävnader sättas i fokus i bilden. Hög energi innebär att mjukvävnad blir "osynlig" och bara material med hög densitet, så som ben eller injicerade kontrastmedel, syns. Låg energi ger bättre bilder av mjukvävnad men på bekostnad av en högre stråldos till patienten, ifall samma bildkvalitet ska erhållas. När tekniken och forskningen går framåt så vill man hela tiden optimera undersökningar, för att bilderna ska ge ett högre diagnostiskt värde och lägre stråldoser. En relativt ny funktion hos datortomografer är "dual energy". Detta innebär att undersökningar görs med två olika energinivåer samtidigt. Med dual energy är det möjligt att separera mellan material som har likartade densiteter men olika sammansättning, och det går även att identifiera specifika material. Vid många undersökningar görs en bildtagning med och utan jodbaserade kontrastmedel. Eftersom jod dämpar röntgenstrålarna olika mycket vid de två energierna så kan man beräkna vad i bilden som är jod. Därefter kan man välja att ta bort jodbidraget vilket skapar en så kallad "virtuell icke-kontrastbild". Ifall metoden är tillförlitlig elimineras behovet av en bildtagning utan kontrastmedel. Detta skulle innebära en direkt reduktion av stråldos till patienten.

I det här arbetet så har just tillförlitligheten i kvantifieringen av jod utretts, och jämförts för två olika datortomografiska kamerasystem med olika metoder för dual energy. Dessa är Somatom Definition Flash (Siemens Healthcare) och IQon Spectral CT (Philips Healthcare). Ett vattenfyllt, cylinderformat fantom användes för att efterlikna en patient. I fantomet placerades olika stora sprutor med olika koncentrationer jodlösning. Därefter togs bilder på fantomet med datortomograferna och ur bilderna mättes jodkoncentrationen. För arbetet studerades jodkoncentrationer likt de som typiskt hittas i blodkärl och i hjärnans mjukvävnad efter en kontrastmedelsinjektion. Resultatet påvisade, för bägge kamerasystemen, att jodkvantifieringen förlorade tillförlitlighet för när lägre jodkoncentration och mindre stora objekt studerades. Detta är viktigt att vara medveten om vid användning av funktioner som utnyttjar jodkvantifiering.

Till sist undersöktes ett potentiellt nytt användningsområde för jodkvantifiering. Frågeställningen var om jodkvantifiering kan användas för att identifiera områden med nedsatt blodförsörjning i hjärnan vid stroke. För en typisk patient dör 2 miljoner hjärnceller varje minut vid stroke, en snabb diagnos och behandling är därför absolut livsviktigt. Vid misstanke om stroke genomförs i dagsläget både en datortomografisk perfusionsundersökning och en angiografi med multifas. I detta arbete undersöktes ifall samma information gick att få ut från angiografin som från perfusionsundersökningen. Trots att bara ett fåtal patienter studerades så gav försöket lovande resultat. Om det visar sig att samma information är tillgänglig så skulle perfusionsundersökningen potentiellt kunna tas bort från rutinen, vilket skulle innebära en nästan halverad stråldos (från cirka 3 till 1,5 mSv) och, kanske viktigast, en snabbare bildtagning.

# Abstract

**Purpose/Background**
Dual Energy Computed Tomography (DECT) have been clinically available for over ten years. Two such systems are currently used at Skane University Hospital (SUS) in Lund. By utilizing materials different attenuating properties at different energies, material decomposition and iodine quantification is possible. The aim of this master thesis was to compare the two DECT systems and determine how the accuracy of iodine quantification is dependent on iodine concentration, size of measured structure and radiation dose, in terms of $CTDI_{vol}$. Furthermore the aim was to develop a method for quantitative evaluation of Multiphase CT Angiography (MP-CTA) using iodine quantification. When there is suspicion of stroke, MP-CTA and CT Perfusion (CTP) are performed. The goal was to find a correlation between MP-CTA and CTP and in extension see if MP-CTA can potentially replace CTP.

**Materials and methods**
A phantom study was performed on two DECT systems; IQon Spectral CT (Philips Healthcare) and Somatom Definition Flash (Siemens Healthcare) using a cylindrical Jaszczak phantom with syringes of different inner diameters (17, 7 and 3 mm) inserted. Syringes were filled with dilutions of contrast material solution (Iomeron® 400 mg I/ml, Bracco Diagnostic Inc.) with iodine concentrations in the interval 0.05 - 14 mg/ml. Scans with radiation doses corresponding to $CTDI_{vol}$ of 2.7, 9.0 and 18.1 mGy were performed to test for potential dose dependence. The deviation in measured iodine concentrations from the true value was studied considering the investigated parameters. For the quantitative evaluation of MP-CTA, on the IQon Spectral CT, a total of seven patients were studied who had CTP and MP-CTA performed. Iodine density as well as HU (corresponding to 70 kVp and mono-energetic 40 keV) was measured as a function of time in vasculatory regions of the brain. The regions were compared between left and right hemisphere and the results were compared to CTP findings.

**Results**
Measurements of iodine concentration showed that the accuracy of the iodine quantification decreased for lower concentrations. Both DECT systems had deviations smaller than 50% for concentrations of 0.88 mg/ml and higher. The root mean square deviation (RMSD) showed less accuracy for smaller syringe diameters; for 17, 7 and 3 mm the RMSD was 0.14, 0.43 and 1.00 for Flash and 0.15, 0.23 and 0.51 for IQon. The IQon was generally more accurate than the Flash. The Flash also had larger variations between successive measurements. RMSD was also higher for $CTDI_{vol}$ of 2.7 mGy as compared to the higher dose levels. Quantitative analysis on MP-CTA showed delayed arrival and excretion of contrast material in the same regions which presented with perfusion deficits for CTP. Difference between healthy tissue and tissue with perfusion deficits was larger for iodine density than for HU.

**Conclusion**
The results of the phantom study was in line with previously performed studies. Iodine quantification is above all highly dependent on the measured concentration. A trend for larger errors with smaller syringe diameter and lower dose level was also found. IQon had a higher accuracy than the Flash, especially for lower iodine concentrations and for smaller syringes. The patient study results showed good correlation between MP-CTA analysis and CTP findings. Results indicate that the MP-CTA can be used to detect perfusion deficits using iodine quantification. The method needs to be further developed and tested in order to see if it can replace CTP.

# Abbreviations

ACA - Anterior Cerebral Artery
AChA - Anterior Choroideal Artery
AICA - Anterior Inferior Cerebellar Artery
CT - Computed Tomography
CTA - Computed Tomography Angiography
CTP - Computed Tomography Perfusion
DECT - Dual Energy Computed Tomography
DLCT - Dual Layer Computed Tomography
DSCT - Dual Source Computed Tomography
FOV - Field of View
HU - Hounsfield Units
LSA - Lenticulo-Striate Arteries
MCA - Middle Cerebral Artery
MP-CTA - Multi Phase Computed Tomography Angiography
SCA - Superior Cerebellar Artery
SD - Standard Deviation
SP-CTA - Single Phase Computed Tomography Angiography
PICA - Posterior Inferior Cerebellar Artery
PCA - Posterior Cerebral Artery
RMSD - Root Mean Square Deviation
ROI - Region Of Interest
VMI - Virtual Mono-energetic Imaging
VNC - Virtual Non Contrast

# Contents

# 1 Introduction

Computed tomography (CT) is a commonly used radiological imaging modality with high diagnostic value at the price of a higher radiation dose, than conventional X-ray imaging for example. In 2005 in Sweden, CT examinations made up 12% of all radiological examinations but contributed to 60% of the collective effective dose to patients. The total number was 650 000 examinations which was a 100% increase since 1995. [1] In 2018 at Skane University Hospital 37% of all radiological examinations were performed on CT and the corresponding number for the whole country is likely of the same order. This means that the use of CT has grown rapidly over the last twenty years and it is likely to continue in the same manner. CT has the benefits of performing quick and highly accurate examinations, being widely available and usable on almost all patients. Because of the need to always optimize examinations, in terms of dose reduction as well as to improve the diagnostic value, there is a lot of research being made in the field.

CT was invented and created in the early 1970's by Sir Godfrey Hounsfield. Dual Energy methods for CT was investigated as early as 1976, by Alvarez and Macovski, but in spite of promising first results the idea of Dual Energy CT was put on hold. It had to wait until the technology had advanced far enough. It was first thirty years later, in 2006, that the Dual Energy CT was a clinical reality. [2, 3] Today, many different methods are clinically available. There are two Dual Energy CTs at Skane University Hospital in Lund, one Dual Layer CT (IQon, Spectral CT, Philips Healthcare) and one Dual Source CT (Somatom Definition Flash, Siemens Healthcare). They both have the ability to, among other things, quantify iodine density but they have different methods for dual energy scanning and material separation.

It is of interest to identify and quantify iodine as most contrast materials today are iodine based. Contrast materials are used in order to create contrast and enable better visibility of, among others, the soft tissue and blood vessels. Iodine quantification is already utilized in applications on the Dual Energy CT system, such as virtual non contrast. Virtual non contrast can be used in dose saving purposes as many scans today are made both without and with contrast. It would be possible to eliminate the first non contrast scan if the contrast material contribution to the image is removed in post-processing. [2] These applications are reliant on the iodine quantification being correct and robust. This leads to the need to investigate the limitations of the two systems, when measuring in small structures or low concentrations.

It is also interesting to investigate futher possibilities for iodine quantification. In the stroke investigatory protocol two examinations called Multi-Phase Angiography CT (MP-CTA) and CT Perfusion (CTP) are performed. Both exams require an individual injection of contrast agent which can be harmful for the kidneys of a patient. A method could be developed for using the contrast uptake in the MP-CTA as a measure of the perfusion in the brain. In the case of stroke, the blood supply to an area of the brain is cut off. It is then important to see if there is a good collateral flow which can keep the tissue viable. If this method works MP-CTA could potentially replace CTP in the stroke investigation in the future. No CTP would mean less contrast agent and the radiation dose to the patient could be approximately cut in half, as typical effective doses for MP-CTA is 1.2-2.4 mSv and for CTP 1.5 mSv.

## 1.1 Aim

The aim of this study is to evaluate the accuracy of iodine quantification and compare two Dual Energy systems, IQon Spectral CT (Philips Healthcare) and Somatom Definition Flash (Siemens Healthcare). This is achieved by studying the dependence of the quantification on iodine concentration and diameter of the measured structure. Iodine concentrations in the interval 14 to 0.05 mg I/ml are studied as these are clinically relevant for brain imaging. Additionally, potential dose dependence on IQon is studied.

The final aim is to investigate if it is possible to do quantitative analysis of the MP-CTA examination, and what method is the best, in order to detect ischemic regions in the brain. The result of the analysis is compared to the patients CTP results in order to establish if the same information is available from the MP-CTA as from the CTP. If MP-CTA can provide the same information as CTP there would be no need for the CTP examination. No CTP would mean one less contrast injection and approximately half the radiation dose (from 3 mSv to 1.5 mSv) to the patient.

# 2 Theory

## 2.1 CT Physics

Computed tomography imaging is performed by acquiring multiple x-ray images with an x-ray source and a detector that rotates around the patient. Since the images are acquired from different angles tomographic reconstruction is possible. A schematic of the computed tomography imaging process is shown in figure 1. In the first step, x-ray images are acquired from a large number of angles. In the second step the acquired projections are sorted into sinograms, one sinogram for each angle and each projection corresponding to a line within a sinogram. In the last step the raw data is used to reconstruct the image data.

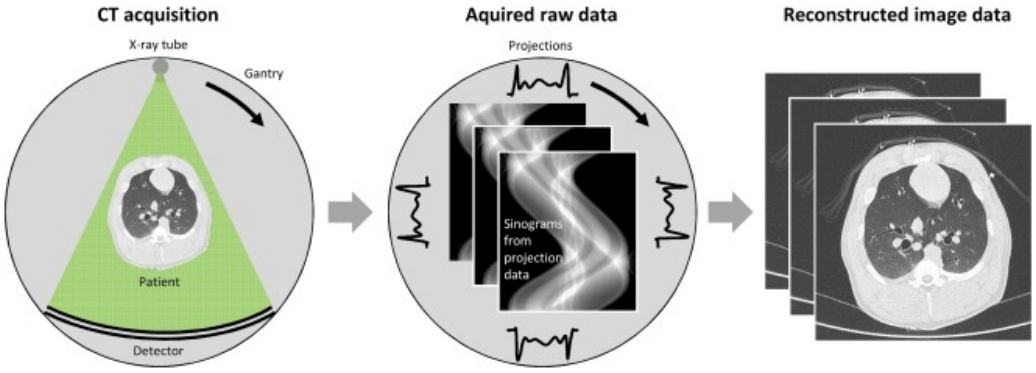


**Figure 1:** Schematic of the computed tomography imaging process. [4]

Although many different reconstruction methods are available there are mainly two categories, filtered back-projection (FBP) and iterative reconstruction (IR). FBP is a simpler method than IR and it takes less time to compute, but artifacts are more frequent and dominant. [5] The image that provide the anatomical information is said to exist in the image domain. By applying a mathematical operation, called the Fourier transform, on the image data it is transformed into the projection domain. In the projection domain image processing is performed with the use of filters, or kernels, in order to enhance the image in various ways, such as reducing the noise level. When the processing is completed the Inverse Fourier transform is applied on the data in order to acquire the anatomical image that is desired.

## 2.2 Dual Energy CT

The Hounsfield Unit (HU) scale is a standardized way of expressing CT numbers. It is obtained using the measured attenuation coefficient in a voxel, $\mu$, and relating it to the attenuation coefficients for water and air, $\mu_{water}$ and $\mu_{air}$, using the relationship in equation (1).

$$HU = 1000 \cdot \frac{\mu - \mu_{water}}{\mu_{water} - \mu air} \tag{1}$$

Due to this definition, water will always have a HU-value of 0 and air a value of -1000. Since the measured attenuation coefficient is not unique for any material, but a function of material composition and density as well as photon energy, this can lead to two different materials being represented in the same HU-value. Or vice versa, same material in different surroundings could have different HU.The material properties cannot be altered in the patient situation, but the photon energy can be varied in order to separate the materials. This leads to the need for Dual

Energy CT (DECT). The basic principle of DECT is utilizing two photon energies, at which materials have different attenuation properties. With this information material differentiation and quantification are possible. Ideally, the two x-ray beams would be monochromatic but that is not possible with the clinical DECT systems currently used. Instead, the manufacturers use different techniques in order to have as little overlap as possible between the high- and low-energetic spectra. [2, 6] Three of the techniques for dual energy scanning are depicted in figure 2, Dual Layer CT (DLCT) and Dual Source CT (DSCT) are further explained in the sections below.

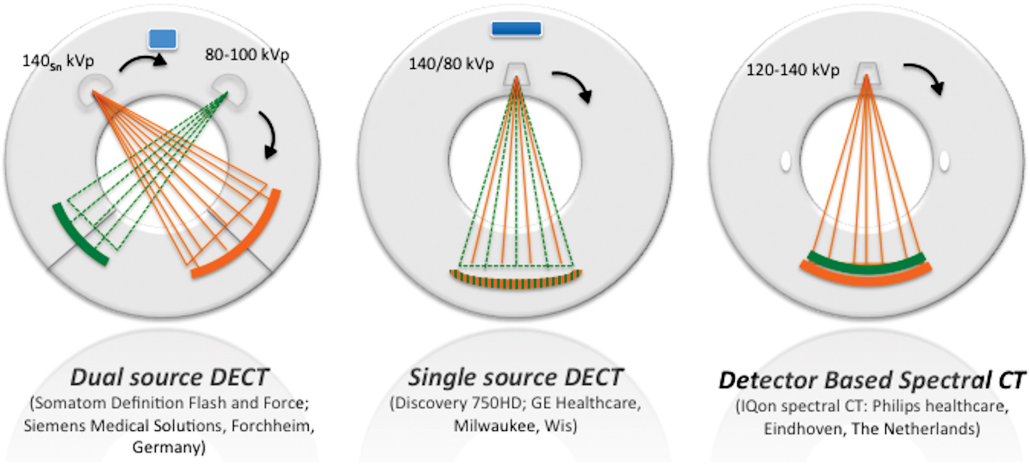


**Figure 2:** Figures of three principles for DECT image acquiring. Left: Dual Source CT with two x-ray sources and two detectors. Middle: Single source CT with one x-ray source (which rapidly switches energy) and one detector. Right: Detector Based Spectral CT (or Dual Layer CT) with one x-ray source and two-layered detector. [7]

### 2.2.1 Dual Layer CT

The DLCT has one x-ray source and a two-layered detector. The low-energetic photons are mainly collected in the top layer while the high-energetic photons are able to pass through the first layer and deposit their energy in the bottom detector. Different thicknesses of the top and bottom layer detector are used in order to get similar noise levels. DLCT has the advantage of simultaneous acquisition of low and high-energy imaging. The downside is that there is a large overlap in the low- and high energy spectra. Also, the noise level may differ for high and low energy spectra due to the amount of low-energy photons differing from the high-energy photons. [2, 6]

### 2.2.2 Dual Source CT

DSCT has two x-ray sources and two detector systems on the same gantry. This allows for independent control of both sources tube potential and current. With DSCT the energy separation between the low and high energy spectra is larger than for DLCT. This creates an improved contrast-to-noise-ratio in the material specific images. A filter can also be used on the high energy tube in order to harden the beam, reducing the lower-energy part of the x-ray spectrum. The downside to DSCT compared to DLCT is that special scatter corrections are needed as scattered photons from one x-ray source may reach the detector of the second x-ray source, this is called cross scatter. There is also a temporal variation between the low and high energetic image acquisition as they are mounted 90 degrees apart on the gantry. [2, 6]

## 2.3 Material Decomposition Algorithms

The dominant interactions, for clinical x-ray energies and materials, which causes the photons to attenuate are the Compton scattering and photoelectric effect. The cross-section for the photoelectric effect is dependent on both the effective atomic number and the X-ray energy while the cross-section for Compton scattering is primarily dependent on the effective atomic number, and not the x-ray energy. The cross-section for the photoelectric effect increases with increasing atomic number and with decreasing x-ray energy. This knowledge is utilized in order to separate materials with DECT. The dependence of these interactions are modeled so that the attenuation of any material can be expressed as a linear combination of two underlying materials. Typically DLCT uses two-material decomposition while DSCT uses three-material decomposition. [2, 8] A simplistic figure of material decomposition is shown in figure 3. Two images are taken at the energies 80 and 140 kV, Material 1 and 2 have similar HU for 80 kV but as they differ considerably for 140 kV they are easy to separate. If the materials are sufficiently different a three material decomposition can be performed. For characterizing unknown materials their HU is mapped onto the plot in order to determine its percentage composition of each of the materials.

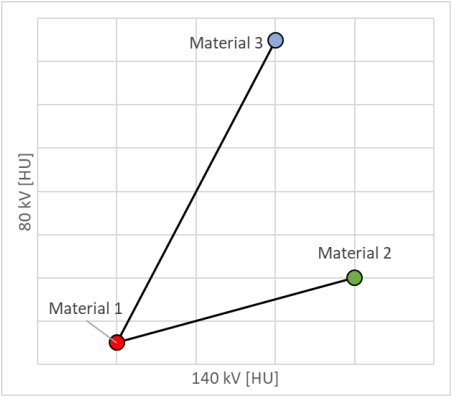


**Figure 3:** A schematic figure of how material decomposition using DECT works.

### 2.3.1 Two-material Decomposition Algorithm

The two-material decomposition algorithm takes place in the projection domain, it analyzes the raw data and generates material specific images. The principle is that two materials are chosen as the material basis pair. The material basis pair can consist of any materials depending on the task at hand. However, the amount of information that can be generated is limited if the two materials have similar attenuating properties. The energy dependence of the attenuation for the two materials are stored in the algorithm. When analyzing the raw data, the algorithm assumes that the signal value in each voxel is a linear combination of the two materials in the material basis pair. Depending on the attenuation in the voxel at the two energies it is decided how much of the voxel can be attributed to each of the two materials. The algorithm produces material specific images when the composition in each voxel is determined. A typical material basis pair is iodine and water. In this case the material specific water image represents the tissues consisting of lower effective atomic numbers and the material specific iodine image represents the higher effective atomic numbers. Substances which have an atomic number between water and iodine, such as calcium, will have a component in both the material specific iodine and water image. [2, 8]

### 2.3.2 Three-material Decomposition Algorithm

The three-material decomposition algorithm takes place in the image domain. A material basis set is used instead of the material basis pair in the two-material algorithm. The material basis set consists of three materials. In order to achieve good results the materials should have separated attenuation properties. Three-material decomposition is possible, even though only two energies are used, under a criteria of mass completeness, meaning that the mass in a voxel has to be the sum of all three mass fractions in the individual material specific images. In principle it first performs a two-material decomposition and the part which don't correspond well with any of them is attributed to the third material. [2, 8]

### 2.3.3 Applications

A useful application on DECT systems is virtual mono-energetic imaging (VMI). These can be created by identifying the contents of a pixel and modeling its attenuation, i.e. photoelectric and Compton interaction cross sections, as a function of energy. VMI has the advantage of decreasing beam-hardening artifacts. There are also applications of iodine quantification on DECT clinically available. By identifying the amount of iodine in voxels it is possible to create an image with a color overlay of the iodinated areas. Another application is virtual non contrast (VNC). With the identification of iodine voxels comes the possibility to remove the iodine components from the image, thus creating a VNC image. If the quality of the VNC is sufficient it can replace the true non contrast (TNC) image in a study. [2, 9] Eliminating the TNC scan would mean a shorter exam time and lower radiation dose to the patient, as well as the advantage of a perfectly matched contrast versus non contrast image set. These applications are dependent on the iodine quantification being correct and robust in order to produce reliable images.

## 2.4 Stroke

Stroke, or cerebral infarction, is the general term for death of brain cells as a result of insufficient oxygenation. This happens when the blood supply to an area of the brain is interrupted, due to a blockage (ischemic stroke) or a bleeding (hemorrhagic stroke). Ischemic and hemorrhagic stroke stand for 85% and 15% of all stroke cases respectively and stroke is one of the leading causes of death globally. [10, 11] As each 1-hour delay in treatment could decrease the odds of good clinical outcome by 38% it is of the utmost importance to diagnose and provide treatment as quickly as possible. [12] Stroke syndrome is characterized by a sudden onset of neurological symptoms. The presenting symptoms vary depending on which region of the brain is affected. The symptoms of ischemic and hemorrhagic stroke are not distinctive enough to enable direct diagnosis, which is why brain and neurovascular imaging is needed in the stroke investigation. [11]

### 2.4.1 Stroke imaging

The current standard for stroke investigations is a non-contrast head CT. Hemorrhagic stroke can be diagnosed with a high accuracy with the non-contrast CT. Major ischemic stroke may also be diagnosed using the non-contrast CT, but it is highly insensitive for detecting minor strokes. [11] Following the non-contrast CT a single-phase CT angiography (SP-CTA) is typically performed in which the arterial filling in the two brain halves are compared. The SP-CTA can tell whether or not there is an intravascular blood clot.

In some cases a perfusion CT (CTP) may be performed. In CTP, images are taken every second for approximately 60 seconds after contrast injection. By analyzing the difference in Hounsfield unit (HU) value, the CTP provides information about the cerebral blood flow (CBF), cerebral blood volume (CBV) and mean transit time (MTT). MTT is the average occupation time for red blood cells within a volume. CTP enables differentiation between salvageable brain tissue, called the penumbra, and irrevocably damaged tissue, the core. The penumbra is the area surrounding the core which has viable brain tissue that suffers from dysfunction and loss of electric activity but has the possibility to recover if treatment is provided in time. [10] The core and the penumbra are characterized by an increased MTT as compared to the normal, healthy tissue. The CBF is reduced in both the core and penumbra but more so in the core. The CBV is the main differentiator between the core and penumbra as it is strongly decreased in the core but normal or increased in the penumbra. [13] It can be debated which threshold values should be used to define penumbra versus core, which will affect the interpretation of the examination. Figure 4 displays an example of how CBV, CBF and MTT looks like in a patient with a large infarcted region in the right hemisphere.

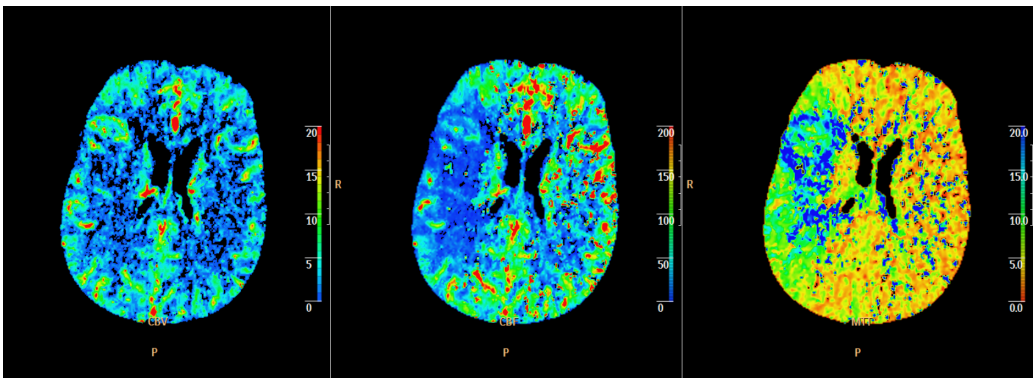


**Figure 4:** CBV, CBF and MTT maps for a patient with a malperfused right hemisphere.
**Left: CBV map**, blue (0 ml/100gm) meaning low and red (20 ml/100gm) meaning high CBV. Map presents no difference between left and right hemisphere, indicating absence of core.
**Middle: CBF map**, blue (0 ml/100 gm tissue/minute) meaning low and red (200 ml/100 gm tissue/minute) meaning high CBF. Right hemisphere has a large region with CBF lower than 50 ml/100 gm tissue/minute, indicating a perfusion deficit.
**Right: MTT map**, red (0 s) meaning short and blue (20 s) meaning long MTT. Map presents a prolonged MTT time in the right hemisphere, indicating a perfusion deficit.

### 2.4.2 Multiphase CT Angiography

Multiphase CT angiography (MP-CTA) is an imaging tool which gives time-resolved information on arterial filling in the brain, unlike SP-CTA. At Skane University Hospital it has replaced the SP-CTA in the clinical stroke protocol. It is used for visually assessing the collateral blood flow. The collateral blood flow can be defined as the artery-to-artery pathways that are able to supply blood to a region of the brain whose primary source of blood has been reduced. [14, 15] In MP-CTA, angiograms of brain vasculature in three phases are generated after injecting contrast material. Images are evaluated by looking at the extent of vessels in the ischemic territory in the symptomatic hemisphere and comparing it to the same region in the asymptomatic hemisphere. [16] Image acquisition is triggered by when the HU in the aorta reaches a specific value. The three phases are timed in order for the first phase to coincide with the peak arterial phase in the normal brain, and the second and third phase with the peak-venous and late-venous phases. In figure 5 the three phases are presented, for the same patient as in figure 4 for the perfusion study. As the patient has damage to the left hemisphere there is a delay in the arrival and excretion of contrast material in the region.

**Figure 5:** Same transversal slice imageof the same patient as in figure 4, for phase 1, 2 and 3. Left: Phase 1. In the right hemisphere there is a large region (encircled) with poor arterial filling. Middle and Right: Phase 2 and 3. Delayed contrast material remain in the region even when as it has left the healthy left hemisphere.

A late venous-phase filling has been shown to be indicative of poor collateral status. Clinical trials have shown that collateral status is highly connected to whether or not reperfusion is successful in the case of intravenous thrombolysis or endovascular intervention. As such it is a a potentially useful tool for predicting outcome as well as for treatment planning. MP-CTA has the advantages of being quick to perform, does not require complex post-processing, requires time and amount of contrast material comparable to SP-CTA and it delivers a lower radiation dose than perfusion studies. [14] Figure 6 shows how a theoretical iodine content could look like in a patient with a healthy hemisphere (right) and a hemisphere with a perfusion deficit (left) if measured in the different phases after injection.

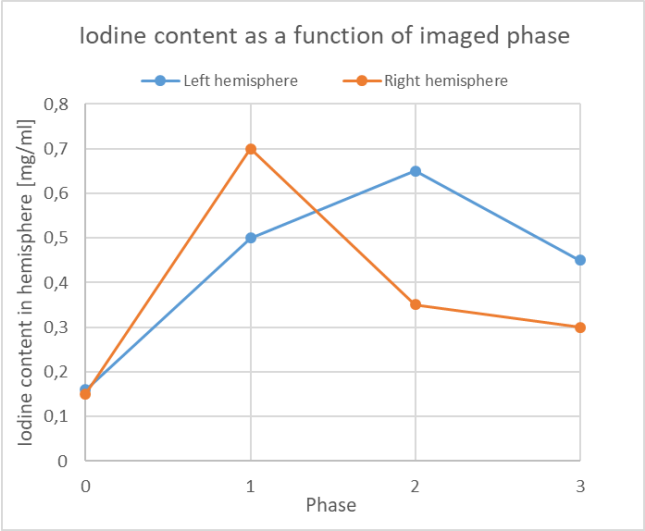


**Figure 6:** The figure shows theoretical examples of normal iodine concentration uptake and retention (red curve/right hemisphere) and example of a hemisphere with interrupted blood supply from e.g a clotted artery (blue curve/left hemisphere).

### 2.4.3 Vasculatory territories in the brain

Figure 7 shows a schematic image of the vasculatory territories in the brain. If there is an occlusion in, for instance, the right Anterior Cerebral artery (ACA) this would result in an interrupted blood supply to the ACA territory, represented in red, on the right side of the brain. Other vasculatory territories in the figure are the Middle Cerebral artery (MCA) in yellow, Posterior Cerebral artery (PCA) in green, Posterior Inferior Cerebellar artery (PICA) in blue, Anterior Inferior Cerebellar artery (AICA) in pink, Anterior Choroideal artery (AChA) in blue, Superior Cerebellar artery (SCA) in white), Lenticulo-striate arteries (LSA) in orange. There are also branches from the vertebral and basilar artery which supplies blood to the medulla oblongata, in blue, and the pons, in green. [17] The MCA territory can be further segmented into smaller regions due to the branching of the artery.

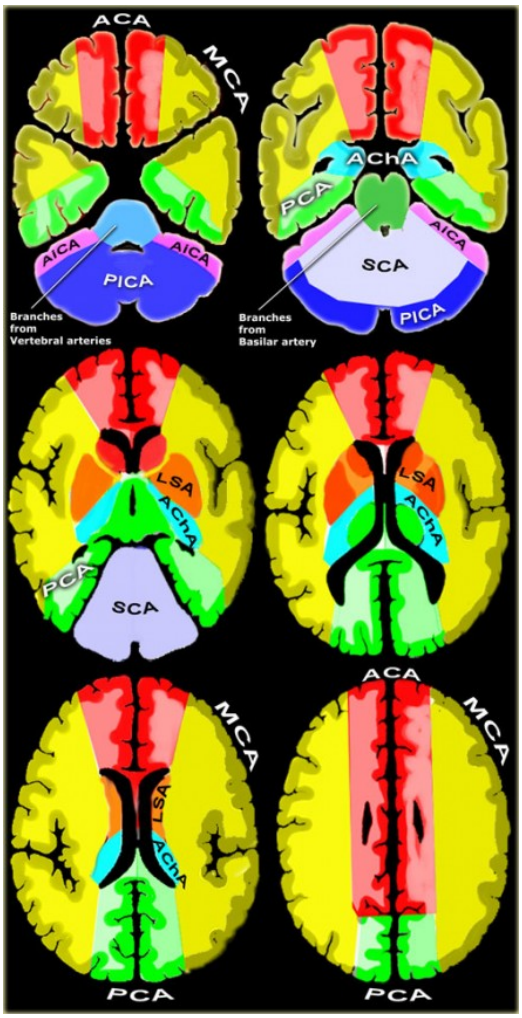


**Figure 7:** Vaculatory territories in the brain, color-mapped after which their main blood supply artery. ACA in red, MCA in yellow, PCA in green, PICA in blue, AICA in pink, AChA in blue, SCA in white, LSA in orange. [17]

# 3 Materials and Methods

## 3.1 Phantom description

The Flanged Jaszczak Phantom is a cylindrical phantom with an inner diameter of 21.6 cm, inner height of 18.6 cm and wall thickness of 3.2 mm. The walls are made of PMMA. [18] The phantom was filled with water and syringes of different inner diameters (17, 7 and 3 mm) were inserted. Different concentrations of iodine solution were produced by diluting contrast material with tap water. The contrast material used was Iomeron® (400 mg I/ml, Bracco Diagnostic Inc.). Iomeron® is an iodine-solution containing the active substance iomeprol and it is administered intravenously. It is commonly used in diagnostics for a variety of x-ray examinations in order to increase the difference in attenuation between structures in the body. The viscosity of it differs from 27.5 mPas at 20$^o$C to 12.6 mPas at 37$^o$C, as compared to water viscosity of 1 mPas. The density is a constant 1.4 g/ml at both temperatures. [19] The solutions were created using hot water (approximately 37-45 degrees), in order to bring down the viscosity of the contrast material, and they were shaken vigorously in each step. A typical patient is injected with around 50-80 ml of contrast material which, assuming a total blood volume of 5 litres and an even distribution of the contrast agent in the blood, would translate to a mean concentration of 4-6.5 mg I/ml. Considering this concentrations of 14, 7, 3.5, 0.88, 0.44, 0.22, 0.11 and 0.05 mg I/ml were studied in the experiment. 100 ml iodine solution with 14 mg I/ml was produced using 96.5 ml (96.5 g) water and 3.5 ml (4.9 g) contrast material. An electronic scale (Mettler Toledo PL601-S) with an $\pm$0.1 g uncertainty was used for the measurement. For the first solution the uncertainty produced an inaccuracy corresponding to $\pm$3%. The following concentrations were created by diluting the first solution 2:1, in each step the concentration uncertainty remained $\pm$3%.

## 3.2 Image acquisition

The DECT systems included in this study were a DLCT (IQon Spectral CT, Philips Healthcare) and a DSCT (Somatom Definition Flash, Siemens Healthcare). The phantom was positioned isocentrically in both CTs as shown in figure 8 and it was centered using the laser positioning system. Measurements on the IQon were made using three exposure levels ($CTDI_{vol}$: 2.7, 9.0, 18.1 mGy) in order to investigate potential dose dependency on the iodine quantification. Three scans were performed for each exposure level and phantom configuration (i.e. iodine concentration). A protocol with acquisition parameters as stated in table 1 was used. The spectral images was reconstructed using iDose4 level 2, Standard (B) filter, matrix size of 512x512, slice thickness 3 mm and 3 mm increment.

**Table 1:** Image acquisition parameters for Philips IQon. Fixed parameters were tube voltage at 120 kV, collimation at 64x0.625 and Field-of-view (FOV) at 380 mm.

| Tube loading [mAs] | $CTDI_{vol}$ [mGy] | Pitch | Rotation time [s] | Scan time [s] |
|---|---|---|---|---|
| 30 | 2.7 | 1.234 | 0.27 | 1.8 |
| 100 | 9 | 1.234 | 0.27 | 2.2 |
| 200 | 18.1 | 1.047 | 0.33 | 3.1 |

A dual energy protocol was used on the Flash with the acquisition parameters stated in table 2. Three scans were performed for each phantom configuration (i.e. iodine concentration). The spectral images were reconstructed using kernel B30f Medium smooth, matrix size of 512x512, slice thickness 3 mm and increment 3 mm.

**Table 2:** Image acquisition parameters for Siemens Flash. Collimation fixed at 128x0.6 and FOV at 300 mm.

| Tube voltage [kV] | Tube loading [mAs] | $CTDI_{vol}$ [mGy] | Pitch | Rotation time [s] | Scan time [s] |
|---|---|---|---|---|---|
| A: 80<br>B: Sn140 | A: 270<br>B: 104 | 9.1 | 0.7 | 0.33 | 3.61 |

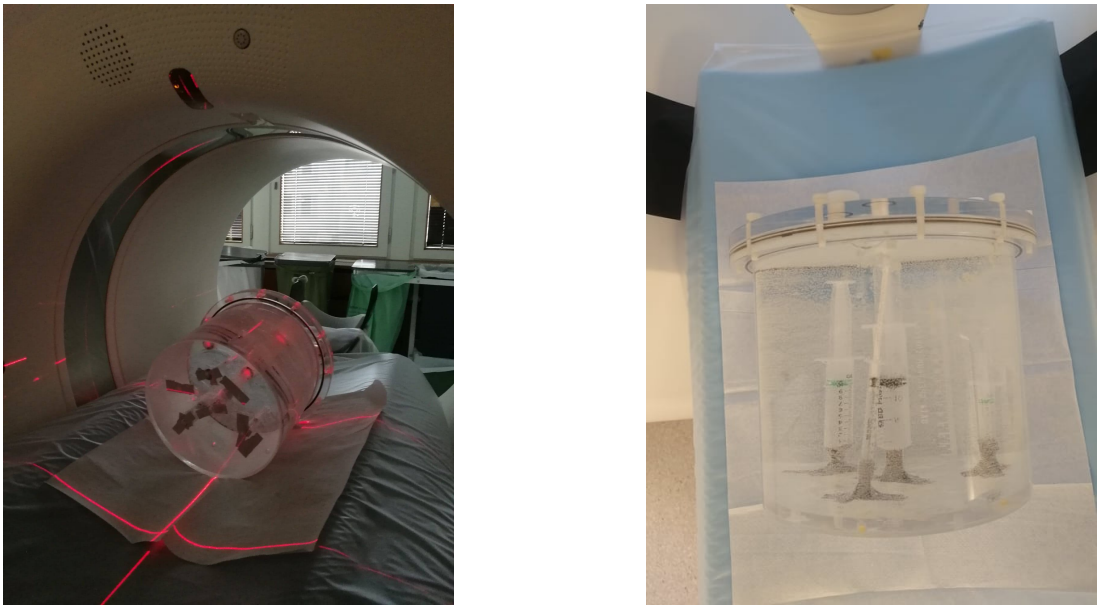

**Figure 8:** Phantom positioning at CT (left) and phantom with syringe inserts (right).

## 3.3 Image analysis

Reconstructed image slices in the transversal direction were analyzed. The program used for analyzing was Philips IntelliSpace for the IQon and Siemens syngo.via for the Flash. Reconstructed images were angled in order for the measured plane to be orthogonal to the central axis of the syringes. ROI (Region of interest) measurements in IntelliSpace were made on the SBI (Spectral Base Images) file using the Iodine Density setting. ROI measurements in syngo.via were made on the Dual Energy file using the Virtual Unenhanced setting. Iodine concentrations were measured in centrally placed ROI and slice thickness of 10 mm. All slices were used except the ends of the syringes, due to artifacts, resulting in an average of 10, 10 and 12 ROIs in each measurement for the 17, 7 and 3 mm syringe. This was repeated for all three scans and the ROI pixel average for each syringe was used as the measured iodine concentration value. The measured ROI area for the 17, 7 and 3 mm syringes were approximately 130, 15, and 2 $mm^2$.

The measured iodine concentration was compared to the true concentration in order to gain a deviation, calculated using equation (2). The deviation as a function of concentration was plotted for all three syringe diameters.

$$Deviation = (Measured/True - 1) \cdot 100 \tag{2}$$

For the comparison between the two systems, the 100 mAs measurement on the IQon and the 270/104 mAs on Flash, both corresponding to a $CTDI_{vol}$ of 9 mGy, was used. Dose dependency was investigated on the IQon using mAs-levels corresponding to $CTDI_{vol}$ of 2.7, 9.0 and 18.1 mGy. The deviation in measured iodine concentration as a function of dose was plotted and analyzed.

The standard deviation of all measurements were estimated using equation (3), in which $x_i$ is the value of each measurement in the sample, $x$ is the mean of the sample and $n$ is the sample size. The standard deviation gives a measure of how much measurements varies from the mean.

$$SD = \sqrt{\frac{\sum_i (x_i - \bar{x})^2}{(n-1)}} \tag{3}$$

## 3.4 Statistical analysis

All statistical analysis was performed in Microsoft Excel. The measured iodine concentrations were analyzed by calculating the Pearson correlation coefficient, $R^2$, with equation 4 for both DECT systems and for all syringe sizes. In the equation $K$ is the number of measurements, $c^i_{obs}$ and $c^i_{true}$ are the observed and true iodine concentration, $\bar{c}_{obs}$ and $\bar{c}_{true}$ are the mean of all measured and all true iodine concentrations respectively. The Pearson correlation coefficient, which provides a measure of the correlation between measured and true iodine concentration, takes a value between -1 and 1. A value of 1 correspond to a strong positive correlation between the two parameters, increase in one means increase in the other, while a value of -1 correspond to a strong negative correlation, increase in one means decrease in the other. If the coefficient has a value close to 0 there is no significant correlation.

$$R^2 = \frac{\sum_{i=1}^{K}(c^i_{obs} - \bar{c}_{obs})(c^i_{true} - \bar{c}_{true})}{\sqrt{\sum_{i=1}^{K}(c^i_{obs} - \bar{c}_{obs})^2}\sqrt{\sum_{i=1}^{K}(c^i_{true} - \bar{c}_{true})^2}}, \qquad c^{i...K} = 0.05, ..., 14 \text{ mg/ml} \tag{4}$$

In order to gain a measure of the overall iodine concentration accuracy of the two DECT systems, the absolute deviation was analyzed by calculating the root mean square deviation (RMSD) between true and measured iodine concentrations. It was calculated using equation 5.

$$RMSD = \sqrt{\frac{\sum_{i=1}^{K}(c^i_{obs} - c^i_{true})^2}{K}}, \qquad c^{i...K} = 0.05, ..., 14 \text{ mg/ml} \tag{5}$$

A two-sample t-test was performed in order to test if the results from the IQon was statistically different from the results of the Flash, for a $\text{CTDI}_{\text{vol}}$-value of 9 mGy. The test was repeated for all iodine concentrations and all syringe sizes, 17, 7 and 3 mm. The null hypothesis was that the differences between their measured means, $\bar{X}$, was equal to zero. The alternative hypothesis was that the difference is larger than zero. The t-test assumes that the dependent variable is approximately normally distributed and continuous. It also should not contain any outliers and each observation needs to be independent of the other. These requirements were all met by the measurements of iodine density. Equation (6) was used for calculating the t-statistic. $n$ represents the sample size, the number of measured ROIs. The standard deviation for the measured iodine density, $SD$, was calculated using equation (3).

$$t = \frac{(\bar{X}_1 - \bar{X}_2)}{\sqrt{\left(\frac{SD_1^2}{n_1} + \frac{SD_2^2}{n_2}\right)}} \tag{6}$$

The Microsoft Excel function "T.DIST.2T" was used which, given the value of the t-statistic, returns the two-tailed Students t-distribution p-value. The p-value gives the probability of obtaining the measured mean under the null hypothesis, a low p-value indicating that the null hypothesis is incorrect. The confidence level was set to 0.05.

## 3.5 Multiphase CT Angiography analysis

Images from MP-CTA are currently only visually assessed and no quantitative measurements are made. The idea for this analysis was to develop a method for measuring iodine concentration, in different vasculatory territories of the brain, as a function of time in order to see if the result can be related to the perfusion exam. The HU-values in the territories were also be analyzed as a function of time as the increased iodine in the brain should correlate to a higher HU-value. Two different kinds of HU was measured, HU corresponding to a x-ray spectra with peak tube voltage 120 kV and HU corresponding to a reconstructed, monoenergetic photon energy of 40 keV. 120 kV was chosen as it is commonly used for patient exams and 40 keV because low photon energies accentuates the contrast agent in the image. Patients were chosen who had both MP-CTA and CTP performed, in order to relate the MP-CTA analysis to the results of the perfusion study.

Seven patients were included in the test, three with a perfusion deficit in the CTP and four without a detected perfusion defect. The patients were examined on IQon Spectral CT using a MP-CTA protocol. Images from phases 1, 2, and 3, as well as the 0-phase, without any contrast, were analyzed in Intellispace using the SBI file. The slice thickness of the images were set to 10 mm. ROIs were drawn after locating the six planes in figure 7, see patient example in figure 10. The measured planes were angled as shown in figure 9a. Plane 5 and 6 were placed above the ventricles as shown in figure 9b. Bone and larger blood vessels were avoided in order to measure the true values of the parenchyma as accurate as possible. The smaller regions, AICA, AChA and PICA (in the second plane), were ignored and included in their neighbouring regions. MCA was divided into M1, M2 and M3 for the 1-4 planes and M4, M5 and M6 for the 5-6 planes. Iodine concentration (obtained using the Iodine Density protocol) and HU (obtained using the "Conventional" protocol, corresponding to 120 kV, and the "Mono-E 40keV" protocol, corresponding to a reconstructed mono-energy of 40 keV) were measured in the ROIs. An average value was used for the regions appearing in more than one plane. The three variables (iodine density, "Conventional"-HU and "Mono-E 40 keV"-HU) were plotted as a function of imaged phase for all regions and compared to the results of the CTP.

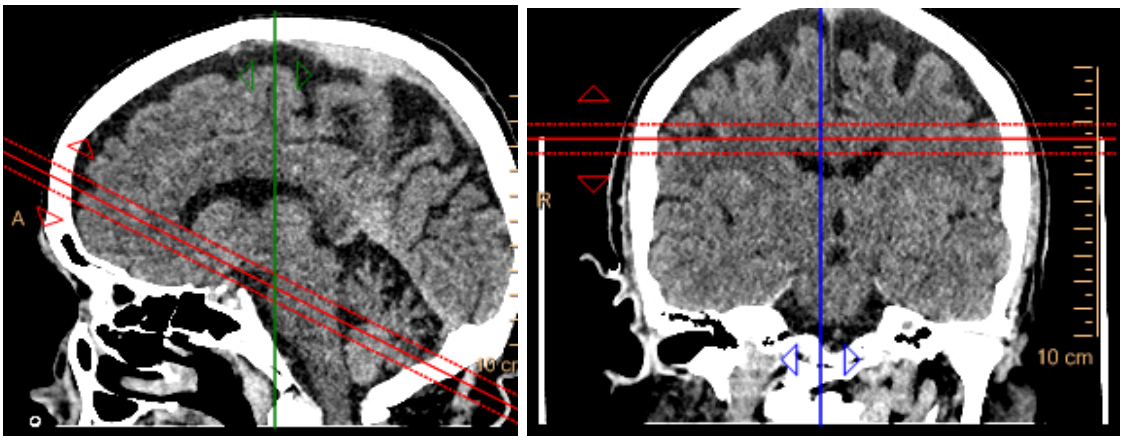


**(a)** **(b)**

**Figure 9:** (a) Figure showing the angle of the measured planes. (b) Figure showing the placement of planes 5 and 6 as they were placed at the top of, or above the ventricles in the figure.

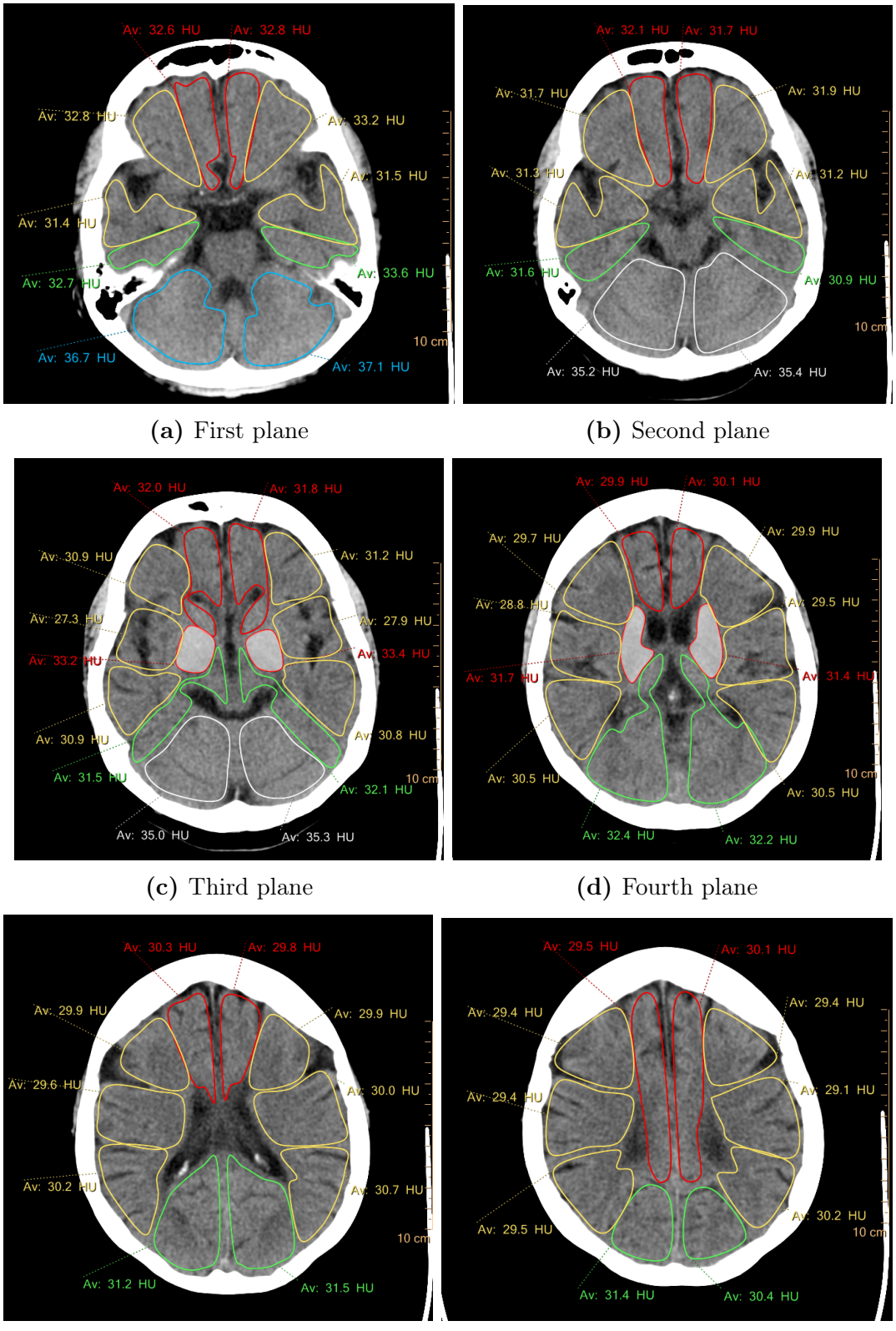


**(a)** First plane **(b)** Second plane

**(c)** Third plane **(d)** Fourth plane

**(e)** Fifth plane **(f)** Sixth plane

**Figure 10:** The six measured planes and regions. Red represents the ACA, yellow the MCA (counting from anterior to posterior; M1-M2 in planes 1-2, M1-M3 in planes 3-4, M4-M6 in planes 5-6), green the PCA, blue the PICA, white the SCA and red edges filled-in with white the LSA.

# 4 Results

## 4.1 Iodine quantification

The numerical deviation from the true iodine concentration is presented in table 3 alongside the corresponding percentage deviation in parenthesis. The percentage deviation as a function of iodine concentration, for all three syringes, is presented in figure 11 for the IQon and figure 12 for the Flash system, with $CTDI_{vol}$ set to 9 mGy. For both systems a trend for larger percentage deviations for lower concentrations are observed. The variability in the measurements also increase for lower iodine concentration, inducing a higher uncertainty. Considering the dependency on structure size, a trend for larger deviation for smaller syringes is observed for both systems. For the lower concentrations, on the Flash, smaller syringe appeared to induce smaller deviations. But these measurements are accompanied by large standard deviations which could be the reason behind this behavior.

Figure 13 shows plots of the measured iodine concentration versus the true iodine concentration for the two systems, IQon to the left and Flash to the right. The top row shows the 17 mm syringe, the second row the 7 mm syringe and the third row the 3 mm syringe. The identity line (i.e. y-intercept = 0 and slope = 1) is shown in orange in each plot. The Flash system tends to overestimate the iodine concentration as the measured values all lie above the identity line and the slope of the linear fits are larger than 1. The IQon system, on the other hand, tends to underestimate the iodine concentration as the slope of the linear fits are smaller than 1. The linear fit is better for larger syringe diameter, most noticeable for the Flash.

**Table 3:** Iodine quantification errors, numerical first and percentage in parenthesis, for IQon and Flash with $CTDI_{vol}$ of 9 mGy.

| | 17 mm | | 7 mm | | 3 mm | |
|---|---|---|---|---|---|---|
| mg I/ml | Flash | IQon | Flash | IQon | Flash | IQon |
| 14.00 | -0.03 (0) | -0.37 (-3) | 0.90 (6) | -0.63 (-5) | 1.26 (9) | -1.13 (-8) |
| 7.00 | 0.31 (4) | -0.02 (0) | 0.72 (10) | -0.05 (-1) | 2.68 (38) | 0.93 (12) |
| 3.50 | 0.06 (2) | 0.05 (1) | 0.35 (10) | 0.00 (0) | 0.42 (12) | -0.21 (-6) |
| 1.75 | 0.14 (8) | 0.27 (15) | 0.44 (25) | 0.26 (6) | 0.40 (21) | 0.05 (3) |
| 0.88 | -0.05 (-12) | 0.11 (13) | 0.23 (32) | 0.15 (17) | 0.19 (33) | -0.20 (-23) |
| 0.44 | -0.16 (-36) | 0.08 (19) | 0.00 (1) | 0.07 (22) | 0.02 (4) | -0.23 (-53) |
| 0.22 | -0.13 (-61) | 0.03 (5) | 0.08 (36) | 0.03 (-2) | -0.02 (-7) | -0.12 (-51) |
| 0.11 | -0.06 (-57) | 0.04 (19) | 0.06 (50) | 0.02 (27) | -0.05 (-41) | -0.03 (-21) |
| 0.05 | -0.06 (-108) | 0.00 (-36) | 0.06 (63) | 0.05 (27) | -0.03 (49) | -0.03 (-68) |

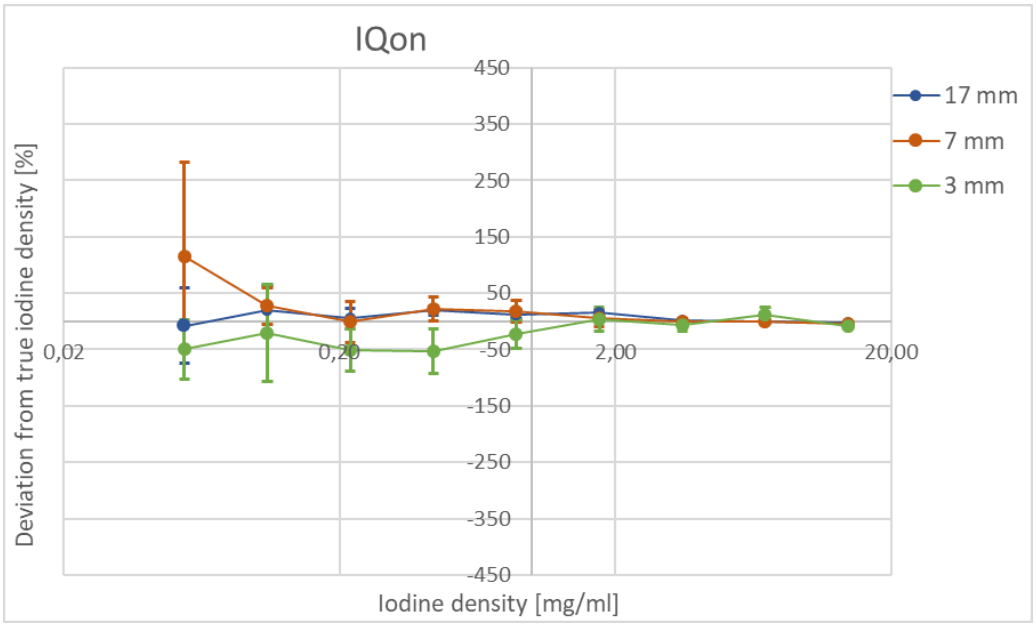


**Figure 11:** The deviation from true iodine concentration as function of iodine concentration for all syringes on the IQon; 17 mm in blue, 7 mm in red and 3 mm in green. The error bars indicate one standard deviation.

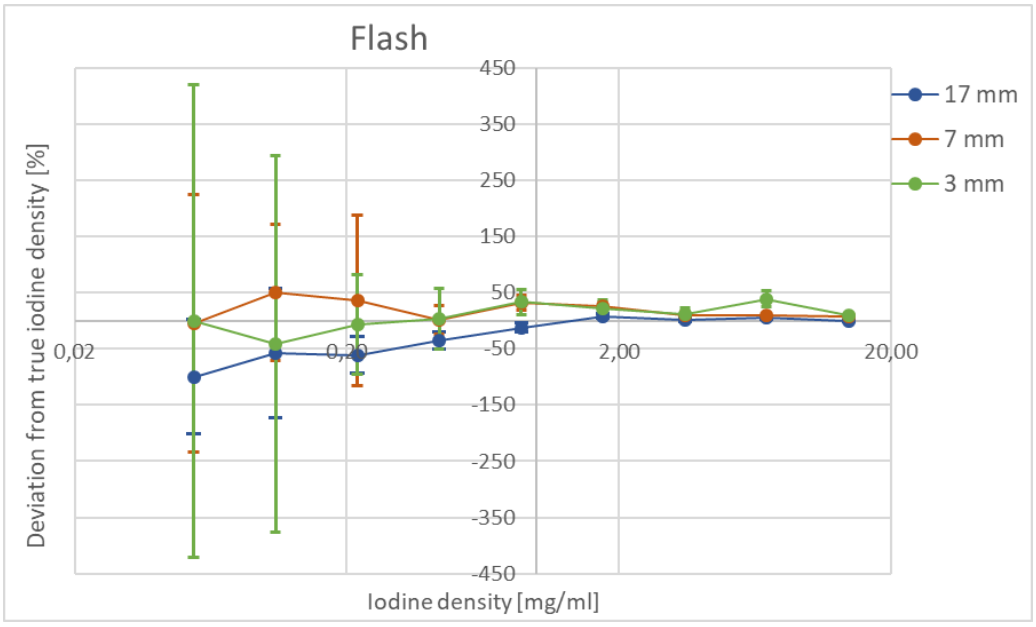


**Figure 12:** The deviation from true iodine concentration as function of iodine concentration for all syringes on the Flash; 17 mm in blue, 7 mm in red and 3 mm in green. The error bars indicate one standard deviation.

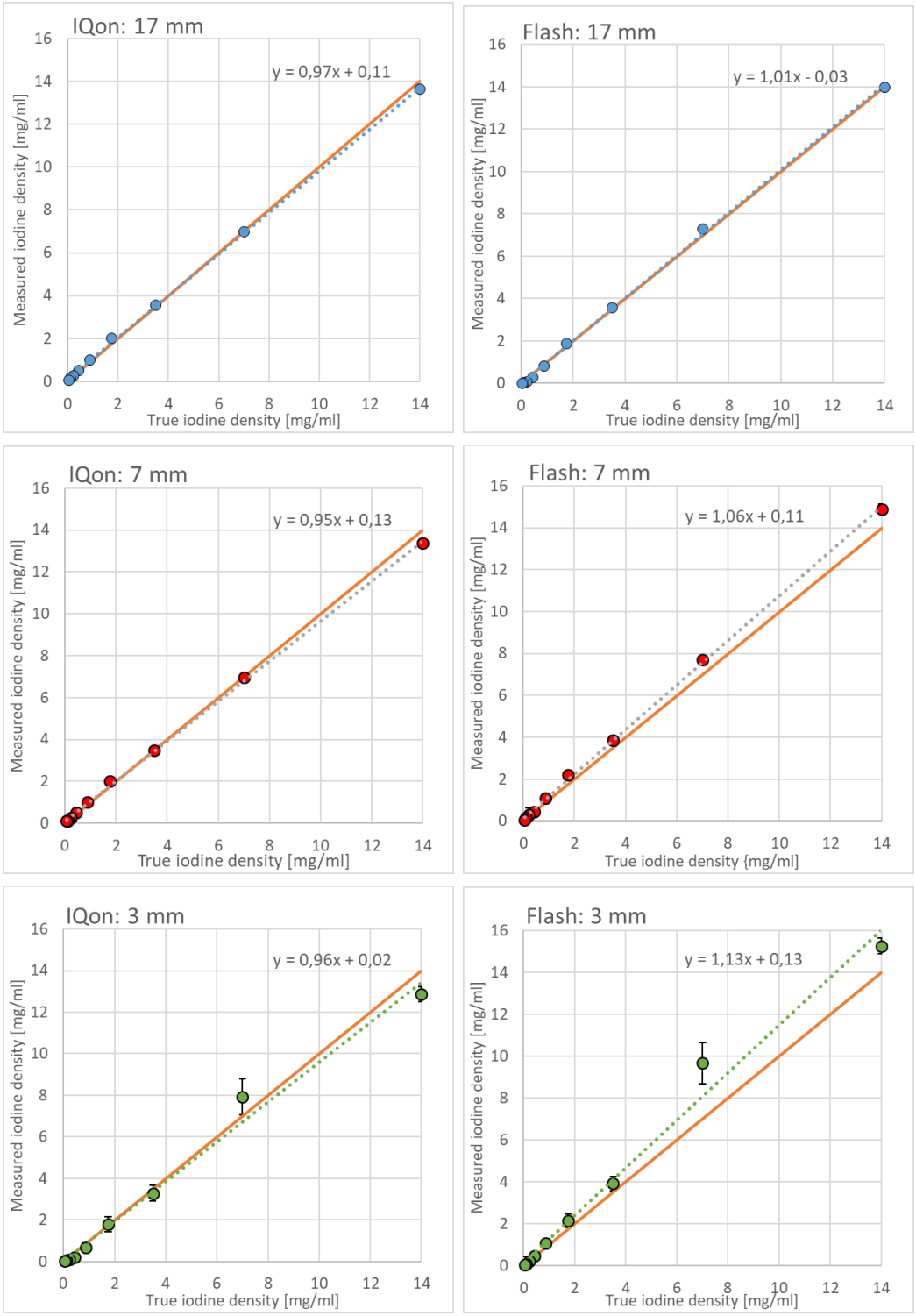


**Figure 13:** Plots of measured versus true iodine concentration for both systems. IQon in the left column and Flash in the right column, with one syringe diameter in each row (17, 7 and 3 mm). Measured iodine concentration is shown as round data points, with error bars indicating one standard deviation, while the identity line is shown in orange. The linear fit to the measured data points is shown as a dotted line and its equation is presented in each figure.

## 4.2 Dose dependency

Dose dependency for measuring iodine concentration with $CTDI_{vol}$-values of 2.7, 9.0 and 18.1 was investigated on the IQon. The percentage deviations as a function of dose, in terms of $CTDI_{vol}$, for three iodine concentrations, 14, 0.88 and 0.22 mg/ml are presented in figure 14 and 15 for the 17, 7 and 3 mm syringe diameter. Only three concentrations are displayed in each plot for simplicity as the rest showed the same behavior. The 14 mg/ml measurements appear to have no dose dependency, regardless of syringe diameter. The mean deviation in the lower concentration measurements, for the 3 and 7 mm syringe, is not constant for all dose levels. This could indicate some dose dependency in the quantification. But, since they also have large error bars the differences in deviations between doses might be over-shadowed by the uncertainty in the measurements.

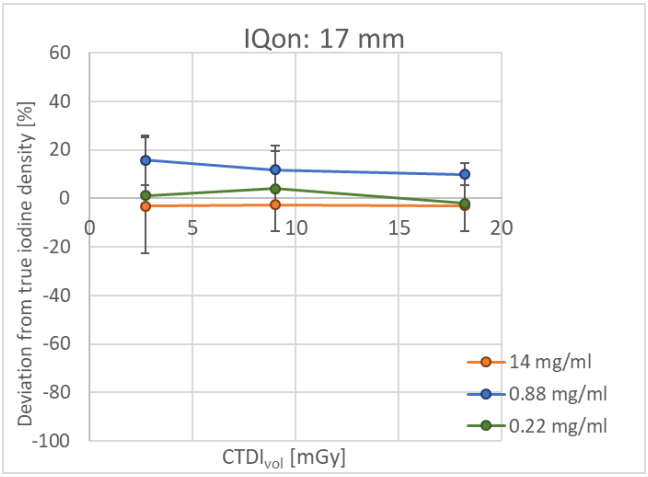


**Figure 14:** Deviation between measured and true iodine concentration as a function of dose level for the 17 mm syringe diameter. The error bars indicate one standard deviation.

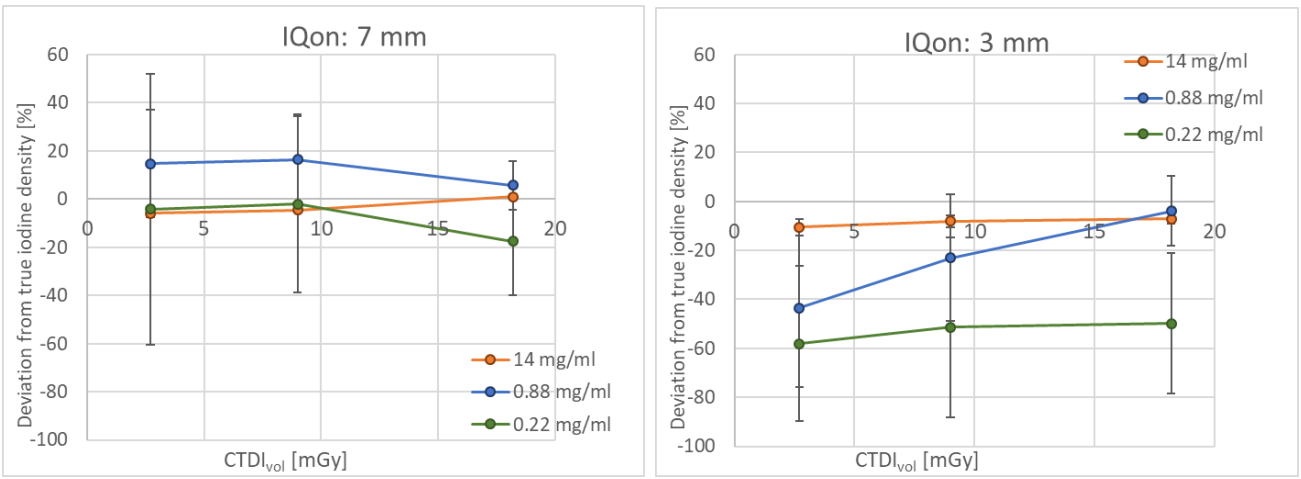


**Figure 15:** Deviation between measured and true iodine concentration as a function of dose level for the 7 mm (left) and 3 mm (right) syringe diameter. The error bars indicate one standard deviation.

## 4.3 Statistical analysis

Pearson correlation coefficient is presented in table 4 for both systems and all syringe sizes. Both systems had strong correlation ($R^2 > 0.99$) all syringe sizes. RMSD for both systems and all syringe sizes is presented in table 5. Comparing the same dose level ($CTDI_{vol}$ of 9 mGy) on the IQon and the Flash, for 17 mm the RMSD is slightly smaller for the Flash. For 7 and 3 mm the Flash has twice as large RMSD as the IQon. As for the dose levels on IQon, there is no difference between $CTDI_{vol}$-values of 9 and 18.1 mGy but for 2.7 mGy the RMSD is slightly higher for all syringe diameters.

The results of the two sample t-test is presented in table 6. p-values lower than 0.05 are marked in bold and the system with the lowest deviation is shown next to it. The systems had a significant difference in their measured values for the majority of the measurements and, in those cases, IQon most often had the lowest deviations from the true value.

**Table 4:** Resulting Pearson correlation coefficients, $R^2$, for all syringe sizes.

| Syringe diameter [mm] | Flash | IQon |
|---|---|---|
| 17 | 0.9996 | 0.9998 |
| 7 | 0.9997 | 0.9997 |
| 3 | 0.9941 | 0.9927 |

**Table 5:** RMSD for all syringe sizes on both DECT sytems and for all dose levels on IQon.

| | Flash | IQon | | |
|---|---|---|---|---|
| $CTDI_{vol}$: | 9 mGy | 2.7 mGy | 9 mGy | 18.1 mGy |
| Syringe diameter [mm] | | | | |
| 17 | 0.14 | 0.19 | 0.16 | 0.16 |
| 7 | 0.43 | 0.28 | 0.23 | 0.23 |
| 3 | 1.01 | 0.57 | 0.51 | 0.49 |

**Table 6:** Resulting p-values of two sample t-test for all syringe sizes (17, 7 and 3 mm) for both DECT systems. p-values lower than 0.05 are marked in bold font and the system with the lowest deviation is presented next to it.

| mg I/ml | 17 mm | | 7 mm | | 3 mm | |
|---|---|---|---|---|---|---|
| 14.00 | **0.00** | Flash | **0.00** | IQon | 0.15 | - |
| 7.00 | **0.00** | IQon | **0.00** | IQon | **0.00** | IQon |
| 3.50 | 0.49 | - | **0.00** | IQon | **0.03** | IQon |
| 1.75 | **0.00** | Flash | **0.00** | IQon | **0.00** | IQon |
| 0.88 | 0.79 | - | **0.00** | IQon | 0.09 | - |
| 0.44 | **0.00** | IQon | **0.00** | Flash | **0.00** | Flash |
| 0.22 | **0.00** | IQon | 0.22 | - | **0.01** | Flash |
| 0.11 | 0.10 | - | 0.32 | - | 0.72 | - |
| 0.05 | **0.00** | IQon | 0.06 | - | 0.58 | - |

## 4.4 Multiphase CT Angiography analysis

Iodine density curves are presented for four patients, two with normal perfusion and two with perfusion deficits. The remaining three patients, not presented, had similar results. Representative vascular territories are presented. For patient 3, with a perfusion deficit, a comparison between the iodine density, "Conventional" and "Mono-E 40 keV"-protocols are also presented. Normal regions are defined as having the same iodine density behavior in left and right side. Deviant regions were defined as having a delayed maximum iodine content as well as or being distinct from their counterpart in the opposite hemisphere.

### 4.4.1 Patients with normal perfusion

#### Patient 1

The patient showed no sign of perfusion deficits on the CTP. Iodine content in all vasculatory regions of the brain were normal, with a maximum iodine density in phase 1 followed by a swift discharge. Iodine density curves for the representative regions are presented in figure 16.

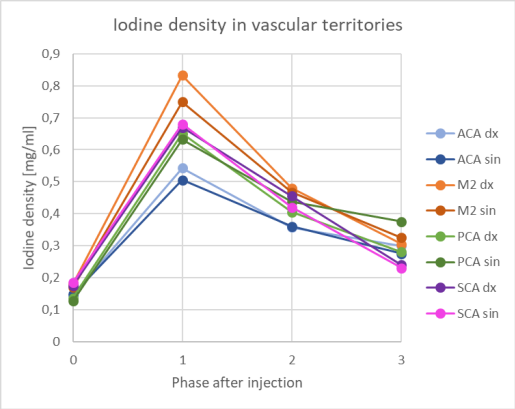


**Figure 16:** Iodine density in ACA, M2, PCA and SCA territories for patient 1.

#### Patient 2

The patient showed no sign of perfusion deficits on the CTP. Iodine content in all vasculatory regions of the brain were normal, with a maximum iodine density in phase 1 followed by a swift discharge. Iodine density curves for the representative regions are presented in figure 17.

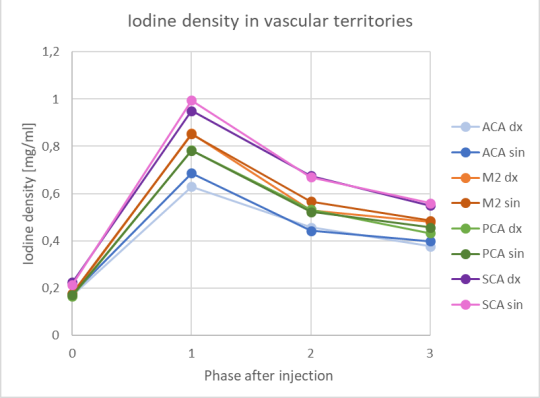


**Figure 17:** Iodine density ACA, M2, PCA and SCA territories for patient 2.

### 4.4.2 Patients with perfusion deficits

**Patient 3**

The CTP results presented perfusion deficits in the whole left MCA territory. The perfusion map, figure 18, showed deficits in the left MCA as well as the left LSA and ACA. No core was detected, only a large penumbra. Iodine density analysis in the PCA, SCA and PICA as well as the whole right hemisphere were normal with maximum iodine density in phase 1. Deviant regions included all the MCA territories as well as ACA and LSA in the left hemisphere which had their maxium iodine density in phase 2 and a prolonged discharge. Figure 19 presents iodine density, as well as "Conventional"-HU and "Mono-E 40 keV"-HU in ACA, PCA and LSA and chosen MCA regions. "Conventional"-HU and "Mono-E 40 keV"-HU show the same behavior as iodine density but less exaggerated.

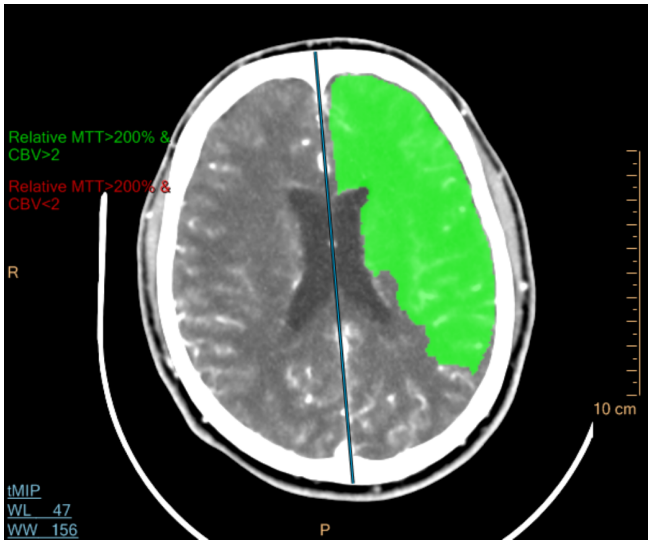


**Figure 18:** Image of patient 3 displaying where perfusion deficits were detected with a color over-lay. Penumbra is shown in green. No core was detected for this patient.

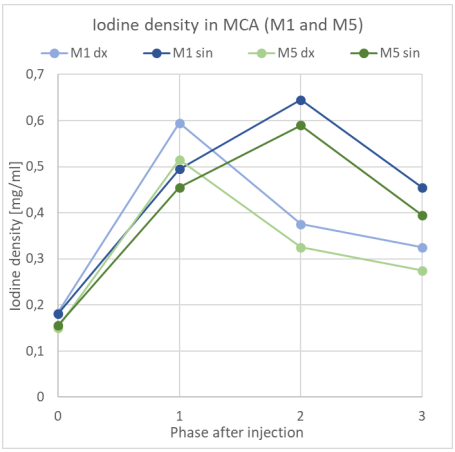


**(a)** Iodine density in MCA (M1 and M5).

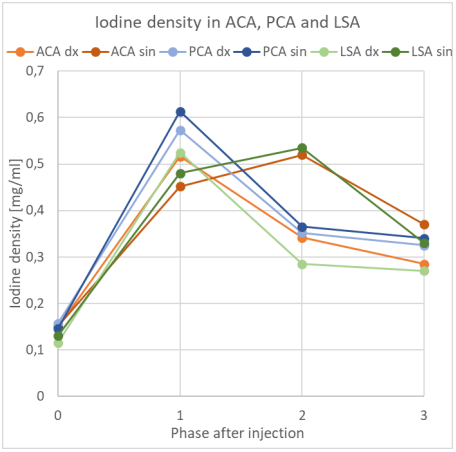


**(b)** Iodine density in ACA, PCA and LSA.

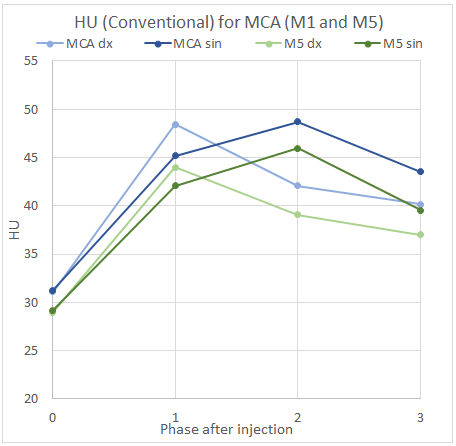


**(c)** "Conventional"-HU in MCA (M1 and M5).

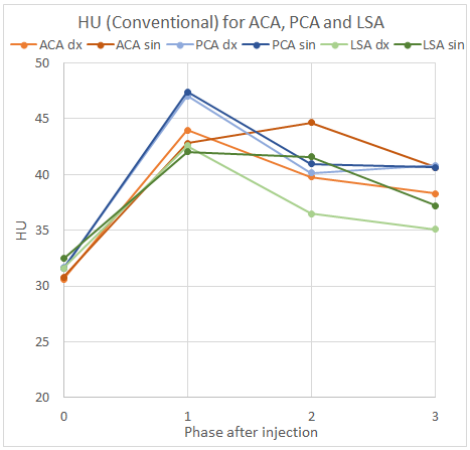


**(d)** "Conventional"-HU in ACA, PCA and LSA.

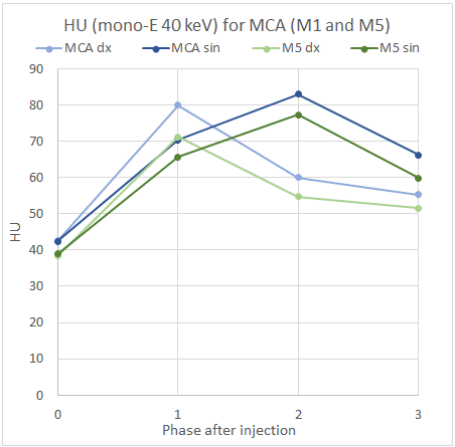


**(e)** "Mono-E 40 keV"-HU for MCA (M1 and M5).

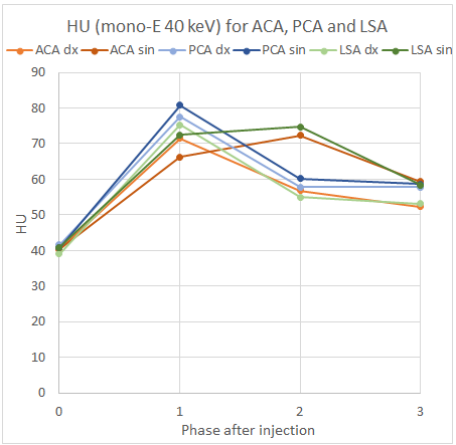


**(f)** "Mono-E 40 keV"-HU for ACA, PCA and LSA.

**Figure 19:** Measurements for patient 3, iodine density in the first row (figure a and b), "Conventional"-HU in the second row (figure c and d) and "Mono-E 40 keV"-HU in the third row (figure e and f). First column (figure a, c and e) shows the MCA territory (M1 and M5), second column (figure b, d and f) shows the ACA, PCA and LSA territory. The curves for M1, M5, ACA and LSA differ in the left and right hemisphere and the maximum value is obtained in phase 2. PCA show a normal behavior in both hemispheres.

### Patient 4

CTP presented perfusion deficits in the whole right MCA. Perfusion map, figure 20 showed deficits in large parts of the right MCA territory without extending into the ACA or PCA. Iodine content analysis showed that deviant regions were all parts of the MCA excluding the M3 region. All other regions were considered normal. Figure 21 presents iodine density in PCA, LSA and SCA (left) and chosen MCA regions (right).

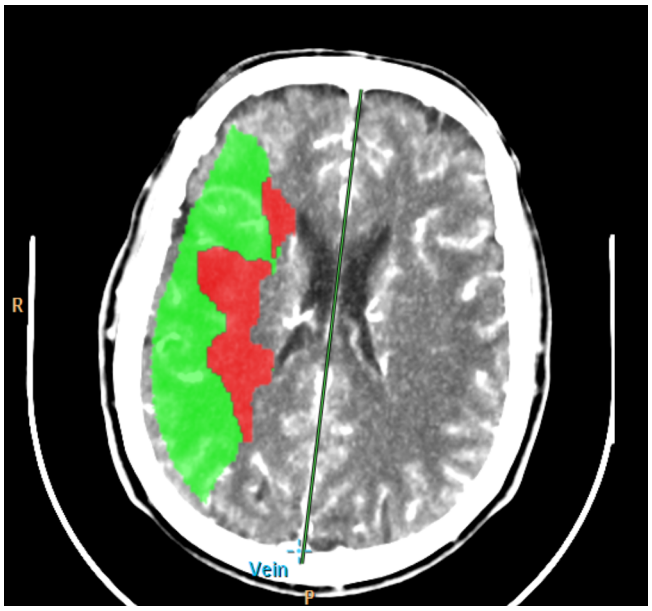


**Figure 20:** Image of patient 4 displaying where perfusion deficits were detected with a color over-lay. Penumbra is shown in green and core in red.

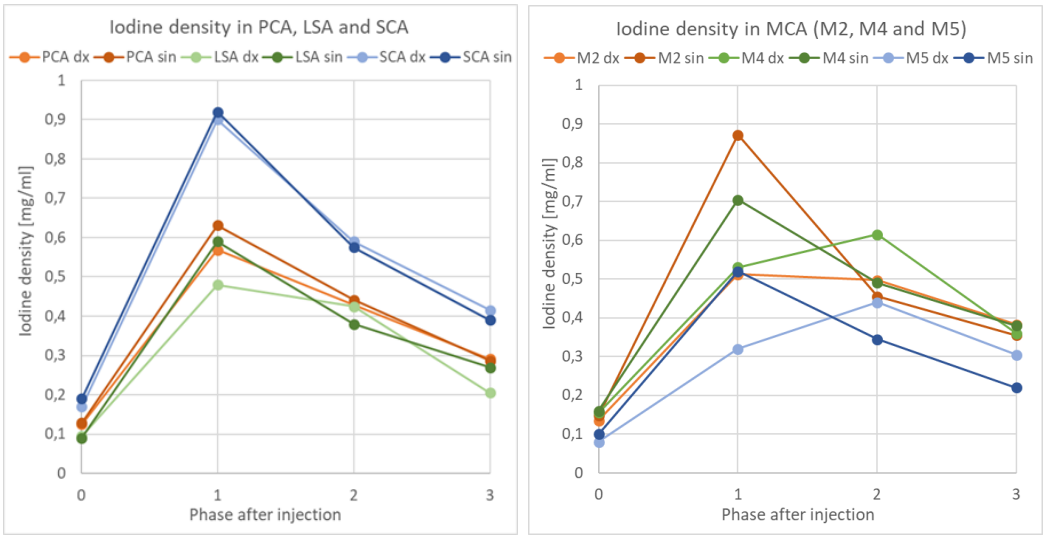


**Figure 21:** Iodine density as a function of imaged phase for PCA, LSA and SCA (left), MCA regions M2, M4 and M5 (right). All MCA territories except M3 exhibited deviant iodine curves with delayed uptake in the left hemisphere and a maximum iodine level in phase 2. PICA, LSA and SCA are normal.

# 5 Discussion

## 5.1 Iodine quantification

### 5.1.1 System comparison

For both DECT systems there was less accuracy, and larger variation between measurements, for lower concentrations of iodine, as can be observed in figures 11 and 12. It is hard to define at which point the uncertainty is so large that the iodine quantification cannot be trusted, and ultimately that depends on for what purpose iodine is measured. The systems had similar deviations from 14 mg/ml and down to 0.88 mg/ml, in this interval the deviation was lower than 50%. Below 0.88 mg/ml the IQon generally had the most accurate iodine quantification, especially considering that the Flash had huge variations in the measurements which is illustrated by the error bars in figure 12. Further supporting that IQon is somewhat superior is the statistical analysis. Table 6 displays for how many measurements the IQon and Flash differed significantly. For the majority of these IQon had the lowest deviation of the two systems. Flash had marginally smaller RMSD for 17 mm (0.14 vs 0.16) while IQon had much smaller RMSD for 7 and 3 mm (0.43 vs 0.23 and 1.00 vs 0.51 respectively). This is also displayed in figure 13, where the IQon had a slope-value closer to 1 for the 7 and 3 mm syringe diameter.

Furthermore, looking at the RMSD, as well as the slope-values in figure 13, shows that the quantification is less accurate for smaller syringe diameters. This is expected as a result of the partial-volume effect, an artifact resulting from the limited resolution of the CT. As a consequence of the FOV and matrix size the resolution in the images are 0.7 and 0.6 mm for the IQon and Flash respectively. Considering that the smallest syringe is only 3 mm in diameter the resolution likely has a large impact on the accuracy of the measurements. When there is more than one material in a voxel the HU, or measured iodine density, will be affected. This makes the edges of the measured object blurry and the placement of ROI, as well as the values of the ROI, less accurate.

In order to compare the two DECT systems their respective scanning och material decomposition methods needs to be discussed. The most important parameter for the performance of material decomposition is the spectral signal-to-noise-ratio (SNR). Spectral SNR is the quota of spectral separation and noise of data sets of each energy spectra, meaning material decomposition can be improved by having a larger energy separation and/or better noise management. It also means that there is a trade-off in the number of energy bins, for the high and low energy data set, and the amount of noise in the images. [2] The Flash, having two separate x-ray sources, has the advantage of a large energy separation. But it also suffers from cross-scatter which influences the noise level in the images. The temporal difference between the two images is also a source of uncertainty. Image based reconstruction, i.e. the Flash system, will also have a larger influence of beam hardening. As the images are acquired with a temporal and spatial variation they need to be reconstructed before material decomposition algorithms can be applied. These reconstructed images are affected by beam hardening, which is likely to degrade the material decomposition. [20] Corrections for beam hardening can be made after the material decomposition but it will not eliminate the artefact fully. The IQon, on the other hand, performs the material decomposition in the projection domain on data free of beam-hardening.

The IQon has the disadvantage of a poorer spectral separation, but it also has the lower noise level of the two DECT systems. Although the details of the material decomposition algorithms for the respective systems are unknown, it is likely a combination of these mentioned effects that causes the observed differences between the systems.

### 5.1.2 Dose dependency

From figure 14 and there was no observable dose dependency. For smaller syringe diameter and/or in combination with low iodine concentration, figure 15, there was a difference between dose levels but due to the high standard deviation it is hard to establish a dose dependency. From the statistical analysis, the RMSD in table 5, it can be seen that the deviation is slightly higher for the lower dose level (2.7 mGy) which supports there being a overall larger uncertainty for lower dose levels. Less accuracy for lower $CTDI_{vol}$-values is expected as this will result in a lower SNR.

### 5.1.3 Earlier works and limitations

The results of this study agrees with previous studies that the two DECT systems can be used to accurately quantify iodine. The accuracy is highly dependent on the measured iodine concentration and the percentage deviation increases for lower concentrations. [21, 22, 23, 24]. Numerically, the results of previous studies and this are not identical but the same trends are observed. The reason for the difference being that the results are highly dependent on phantom configuration and scanning protocol. As for the comparison between IQon and Flash, a previous study by Soesbe et al. (for iodine concentrations in the interval 0-6 mg/ml) is in support that the Flash system is less accurate than the IQon. Similarly to what was found in this study, a tendency to overestimate iodine concentration was typical for the Flash while IQon more often underestimates it. [22] In contrast, a study by Chandarana et al. did not present this overestimation for the Flash. [24] Considering the dose depedency, a tendency for less accurate iodine quantification for lower $CTDI_{vol}$-values was established by Sauter et al. The study in question compared the accuracy for $CTDI_{vol}$-values for 2.5, 5, 10 and 20 mGy (iodine concentrations in the interval 1-10 mg/ml) and found the 10 and 20 mGy scans to be similar while 2.5 and 5 mGy were less accurate. [21]

This study has limitations that needs to be addressed. The uncertainty in the concentration, of the dilutions of iodine solution, was estimated as $\pm 3\%$ due to limitations in the scale that was used. This will have an effect on all of the presented deviations. Measurements were performed in a phantom and not in a patient. Accuracy of iodine quantification would, in the patient situation, be affected by patient movement, size and eventual implants (beam hardening) as well as the fact that there is a background level of iodine in the tissue. Scanning parameters also influences the accuracy of the iodine quantification, for example tube voltage which determines the size of the spectral separation. Further investigation is needed to determine the optimal scan protocol for iodine quantification in the patient situation. To achieve this future studies with an anthropomorphic phantom is proposed.

## 5.2 Multiphase CT Angiography analysis

Even for radiologists with years of training it can be difficult to identify the regions of the brain with certainty on CT. Furthermore, the variation between patients is big. As a physicist, with little starting knowledge of the brain anatomy and experience with looking at CT images, this was a challenge and consultation by radiologists when drawing the ROIs was necessary. Even so, it may be a source of uncertainty in the placement of the ROIs. These results should be seen as an indicator of the potential of iodine quantification in brain imaging and for detecting ischemic areas. The method used produces an estimate of in which vascular territories of the brain deviant blood supply exists in. A risk with this method is averaging out abnormalities, if only part of the region is ischemic, making it appear as though it has normal function.

As was established in the phantom study, there is a relatively large uncertainty when measuring iodine density. For the observed patients the iodine density was between 0.2 and 0.9 mg/ml. It can be seen in table 3 that the mean deviation in this interval, for IQon, lies around 0.0-0.2 mg/ml. This uncertainty induces a risk for false results as the difference between normal and ischemic regions was only approximately 0.2-0.3 mg/ml. However, in the patient situation the relative iodine density, left versus right hemisphere, is of interest and not the absolute measure of iodine density.

### 5.2.1 Correlation with CTP

The result of this study indicates a probable correlation between iodine density analysis and CTP, i.e. between deviant regions in the iodine density analysis and perfusion deficits detected with CTP. All observed patients, both ones presented and not presented in the results, without a perfusion deficit displayed near identical iodine density curves in left and right hemisphere while all patient with a perfusion deficit had deviant iodine density curves in some or all of the regions with perfusion deficits on the CTP. As only seven patients were available, due to MP-CTA being relatively new and not all patients perform both MP-CTA and CTP, future studies should include a larger number of patients in order to verify the method. It would be interesting to perform the same analysis on voxel level in order to create a more sensitive map of where perfusion deficits exists. In order to create such a program at least three obstacles need to be overcome. First, an image registration is needed, registering the image from the non-contrast scan (phase 0) and the three images from the MP-CTA (phase 1-3) in the same coordinate system. Secondly, a pair-wise voxel registration of left and right hemisphere in order to compare the iodine density. Third, a mathematical definition of a perfusion deficit for tissue in terms of iodine content needs to be decided. Even though it appears likely that MP-CTA analysis can be used to replace CTP in terms of detecting perfusion deficits, further investigation is needed in order to determine if it can be used to distinguish salvageable tissue, i.e. penumbra and core. Before CTP can be eliminated a method for such distinction needs to be developed.

### 5.2.2 Iodine density or Hounsfield units

All protocols ("Conventional"-HU, Iodine density and "Mono-E 40 keV"-HU), see figure 19, presented the same shape and behavior as functions of time. They are, however, more expressed for the iodine density protocol. As a result of this iodine density is likely the most sensitive of the three protocols for detecting perfusion deficits. The ratio between ischemic and healthy regions is larger for iodine density, 1.7, compared to 1.1 and 1.4 for "Conventional" and "Mono-E 40 keV", respectively. The "Mono-E 40 keV" protocol has a larger difference than the "Conventional" which is expected since a lower energy amplifies the signal from the contrast agent. The HU value gives a measure of the density in the measured region, which will increase slightly with the arrival of the contrast agent, but iodine density looks only at the contrast agent. There is no iodine in the brain, causing the iodine density curve to start at a relatively low value as compared to the HU curves. Looking at figure 19, the relative increase from starting to peak value is as large as 3.2 for iodine density while only 1.6 and 2.0 for "Conventional" and "Mono-E 40 keV" respectively.

### 5.2.3 Variation in patients

Selected patients were presented in the results, whose iodine density curves had its maximum in phase 1 in the healthy brain. For other patient cases (not presented in this report), both with and without perfusion deficits, the iodine reached the peak value in phase 2 for the healthy brain. For all healthy regions the left and right side was identical and for the regions with perfusion deficits there was further delay, causing the deficit to still be detectable. As such the results were the same, only delayed by a phase, and could still be correlated to the CTP results. This delay could be caused by a weaker heart function in these patients. Slower time from injection to trigger point in aorta for these patients support this theory. Another reason could be the timing of the acquisition. Phase 1 should theoretically be the peak arterial phase, but that does not necessarily correspond to maximum amount of contrast material in parenchyma. The maximum can thus be found in either phase 1 or 2 or sometime in between the phases. One patient had less expressed perfusion deficits than for the ones presented, manifesting not in the whole vascular regions but in a smaller part. For this patient there was a delay of iodine arrival and excretion in the effected regions, although not as distinct as for the patients with larger regions of perfusion deficit. This is likely due to the previously mentioned insensitivity of the method which comes from measuring in large regions.

# 6 Conclusion

In this study the accuracy of iodine quantification for two DECT systems, IQon Spectral CT and Somatom Definition Flash was investigated, as well as how the quantification is influenced by iodine concentration and size of structure. Although both systems were capable of identifying iodine for concentrations as low as 0.11 mg/ml, there was a clear trend for larger deviations for lower concentrations of iodine. The Flash generally had larger errors than the IQon and in particular the variations between measurements were large for the Flash. Measuring on smaller structures resulted in larger errors. Slightly less accuracy was detected for $CTDI_{vol}$ of 2.7 mGy than for 9.0 and 18.1 mGy, indicating a dose dependency in the iodine quantification. It should however be noted that doses that low is not commonly used.

A correlation between regions with perfusion deficits detected with CTP and deviant iodine density curves in MP-CTA was found. Both iodine density and HU can be used but iodine density gave the best results. The method can be used for detecting abnormalites quantitatively and it would likely be more sensitive if performed on voxel level. Wheather or not the MP-CTA can replace the CTP in terms of distinguishing between salvageable tissue or not has yet to be investigated. If the MP-CTA could replace the CTP it would mean an approximate 50% reduction in radiation dose to the patient as well as less strain on the kidneys due to the extra dose of contrast material. And most importantly, if the same information can be gained from the MP-CTA as the CTP precious time can be spared. As brain cells die rapidly after a stroke it is essential to have an effective stroke protocol.

# 7 Future prospects

The results from the MP-CTA analysis showed good correlation between MP-CTA and CTP results. However, due to the variation between patients a larger amount of patient data should be analyzed with the method in order to attain reliability. Also, a voxel-wise calculation of the iodine density content is proposed as it would be more sensitive. The ideal way to present the result would be, not in curves, but as color-maps similar to the perfusion results so that it can be easily interpreted by a radiologist. A challenge still remains in constructing a method for voxel-wise identification of abnormality. First, a co-registration of the images from the four phases in the same coordinate system is needed. For each image a registration between voxels in left and right hemisphere is required. Finally, threshold values for what difference between left and right hemisphere is considered normal/deviant needs to be defined. If the MP-CTA analysis is to replace the CTP a way to distinguish salvageable tissue, penumbra, needs to be developed as well. In order to create such definitions a much larger number of patients need to be included for further studies.

# 8 Acknowledgements

Specials thanks goes to all that have helped me complete my master thesis,

**Kristina Ydström**, thank you for all the ideas and encouragement along the way as well as your outstanding enthusiasm.

**Johan Wasselius** and **Helena Mellander**, thank you for your physiological expertise and for providing information and help on the medical perspective.

**Department of Clinical Physiology and Cecilia Hindorf**, thank you for the helpful advice and for providing the phantom and equipment needed.

**All personnel on IQon (lab 36) and Flash (lab 2)**, thank you for your cooperation and support during my many measurements.

# References

[1] Almén A, Richter S, Leitz W. Radiologiska undersökningar i Sverige under 2005 [Internet]. Stockholm: Statens Strålskyddsinstitut (Strålsäkerhetsmyndigheten); 2008. SSI Rapport; 2008:03 [cited 2019 Mar 25];Available from: https://www.stralsakerhetsmyndigheten.se/contentassets/110d080715414b1c9bea2a9217c151e2/200803-radiologiska-undersokningar-i-sverige-under-2005.

[2] McCollough CH, Leng S, Yu L, Fletcher JG. Dual- and Multi-Energy CT: Principles, Technical Approaches, and Clinical Applications. Radiology. 2015;276(3):637–653. PMID: 26302388. Available from: https://doi.org/10.1148/radiol.2015142631.

[3] Graser A, Johnson TRC, Chandarana H, Macari M. Dual energy CT: preliminary observations and potential clinical applications in the abdomen. European Radiology. 2008 Aug;19(1):13. Available from: https://doi.org/10.1007/s00330-008-1122-7.

[4] Stiller W. Basics of iterative reconstruction methods in computed tomography: A vendor-independent overview. European Journal of Radiology. 2018;109:147 – 154. Fig. 1. Simplified schematic of the imaging process from data acquisition to image reconstruction in (spiral) computed tomography (CT); p. 148. Available from: http://www.sciencedirect.com/science/article/pii/S0720048X18303747.

[5] Stiller W. Basics of iterative reconstruction methods in computed tomography: A vendor-independent overview. European Journal of Radiology. 2018;109:147 – 154. Available from: http://www.sciencedirect.com/science/article/pii/S0720048X18303747.

[6] Forghani R, Man BD, Gupta R. Dual-Energy Computed Tomography: Physical Principles, Approaches to Scanning, Usage, and Implementation: Part 1. Neuroimaging Clinics of North America. 2017;27(3):371 – 384. Dual Energy CT: Applications in Head and Neck and Neurologic Imaging. Available from: http://www.sciencedirect.com/science/article/pii/S1052514917300187.

[7] Patino M, Prochowski A, Agrawal MD, Simeone FJ, Gupta R, Hahn PF, et al. Material Separation Using Dual-Energy CT: Current and Emerging Applications. RadioGraphics. 2016;36(4):1087–1105. Fig. 2. Representation of three commercially available approaches for DE CT scanning. PMID: 27399237. Available from: https://doi.org/10.1148/rg.2016150220.

[8] Patino M, Prochowski A, Agrawal MD, Simeone FJ, Gupta R, Hahn PF, et al. Material Separation Using Dual-Energy CT: Current and Emerging Applications. RadioGraphics. 2016;36(4):1087–1105. PMID: 27399237. Available from: https://doi.org/10.1148/rg.2016150220.

[9] Forghani R, Man BD, Gupta R. Dual-Energy Computed Tomography: Physical Principles, Approaches to Scanning, Usage, and Implementation: Part 2. Neuroimaging Clinics of North America. 2017;27(3):385 – 400. Dual Energy CT: Applications in Head and Neck and Neurologic Imaging. Available from: http://www.sciencedirect.com/science/article/pii/S1052514917300199.

[10] Vilela P, Rowley HA. Brain ischemia: CT and MRI techniques in acute ischemic stroke. European Journal of Radiology. 2017;96:162–172. Available from: http://www.sciencedirect.com/science/article/pii/S0720048X17303339.

[11] Musuka TD, Wilton SB, Traboulsi M, Hill MD. Diagnosis and management of acute ischemic stroke: speed is critical. CMAJ. 2015;187(12):887–893. Available from: http://www.cmaj.ca/content/187/12/887.

[12] Menon BK, Almekhlafi MA, Pereira VM, Gralla J, Bonafe A, Davalos A, et al. Optimal Workflow and Process-Based Performance Measures for Endovascular Therapy in Acute Ischemic Stroke. Stroke. 2014;45(7):2024–2029. Available from: https://www.ahajournals.org/doi/abs/10.1161/STROKEAHA.114.005050.

[13] Krishnan PM, Murphy AM, Aviv RIM. CT-based Techniques for Brain Perfusion. Topics in Magnetic Resonance Imaging. 2017 Jun;26(3):113–119. Available from: https://doi.org/10.1097/RMR.0000000000000129.

[14] Ginsberg MD. The cerebral collateral circulation: Relevance to pathophysiology and treatment of stroke. Neuropharmacology. 2018;134:280 – 292. Cerebral Ischemia. Available from: http://www.sciencedirect.com/science/article/pii/S0028390817303702.

[15] Cipolla MJ. The Cerebral Circulation. Chapter 2, Anatomy and Ultrastructure. San Rafael (CA): Morgan Claypool Life Sciences; 2009;Available from: https://www.ncbi.nlm.nih.gov/books/NBK53086/.

[16] Menon BK, d'Esterre CD, Qazi EM, Almekhlafi M, Hahn L, Demchuk AM, et al. Multiphase CT Angiography: A New Tool for the Imaging Triage of Patients with Acute Ischemic Stroke. Radiology. 2015;275(2):510–520. Available from: https://doi.org/10.1148/radiol.15142256.

[17] Smithuis R. Brain Ischemia - Vascular territories [Internet]. The Netherlands: Radiology department of the Alrijne Hospital in Leiderdorp; 2008 [cited 2019 May 20];Available from: http://radiologyassistant.nl/en/p484b8328cb6b2/brain-ischemia-vascular-territories.html.

[18] Data Spectrum Corporation. Flanged Jaszczak ECT Phantoms [Internet]. Data Spectrum Corporation; 2007 [cited 2019 May 16];Available from: http://www.spect.com/pub/Flanged_Jaszczak_Phantoms.pdf.

[19] FASS Allmänhet. Iomeron [Internet]. FASS Allmänhet; 2018 [cited 2019 Feb 08];Available from: https://www.fass.se/LIF/product?userType=2&nplId=19971017000100&docType=6&scrollPosition=0.

[20] Winklhofer S, Lambert JW, Sun Y, Wang ZJ, Sun DS, Yeh BM. Pelvic Beam-Hardening Artifacts in Dual-Energy CT Image Reconstructions: Occurrence and Impact on Image Quality. American Journal of Roentgenology. 2017;208(1):114–123. Available from: https://www.ajronline.org/doi/pdf/10.2214/AJR.16.16013.

[21] Sauter AP, Kopp FK, Münzel D, Dangelmaier J, Renz M, Renger B, et al. Accuracy of iodine quantification in dual-layer spectral CT: Influence of iterative reconstruction, patient habitus and tube parameters. European Journal of Radiology. 2018;102:83 – 88. Available from: http://www.sciencedirect.com/science/article/pii/S0720048X18300901.

[22] Soesbe TC, Ananthakrishnan L, Lewis MA, Duan X, Nasr K, Xi Y, et al. Pseudoenhancement effects on iodine quantification from dual-energy spectral CT systems: A multivendor phantom study regarding renal lesion characterization. European Journal of Radiology. 2018;105:125 – 133. Available from: http://www.sciencedirect.com/science/article/pii/S0720048X18302067.

[23] Pelgrim GJ, van Hamersvelt RW, Willemink MJ, Schmidt BT, Flohr T, Schilham A, et al. Accuracy of iodine quantification using dual energy CT in latest generation dual source and dual layer CT. European Radiology. 2017 Sep;27(9):3904–3912. Available from: https://doi.org/10.1007/s00330-017-4752-9.

[24] Chandarana H, Megibow AJ, Cohen BA, Srinivasan R, Kim D, Leidecker C, et al. Iodine Quantification With Dual-Energy CT: Phantom Study and Preliminary Experience With Renal Masses. American Journal of Roentgenology. 2011;196(6):W693–W700. Available from: https://www.ajronline.org/doi/full/10.2214/AJR.10.5541.